CDF/PHYS/TOP/PUBLIC/9025

Top Mass Measurement in the Lepton + Jets Channel Using a Modified Matrix Element Method and *in situ* Jet Calibration with 1.7 fb^{-1}

The CDF Collaboration
URL http://www-cdf.fnal.gov
(Dated: September 28, 2007)

We report a measurement of the top quark mass obtained from $p\bar{p}$ collisions at $\sqrt{s} = 1.96$ TeV at the Fermilab Tevatron using the CDF II detector. We calculate a signal likelihood using a matrix element integration method. "Effective propagators" are employed to take into account the effect of simplifying assumptions used in the analysis of the event kinematics. We use a neural network discriminant to distinguish signal from backgrounds. Our overall signal probability is a 2-D function of $M_{\rm top}$ and the jet energy scale (JES), where JES is a multiplicative factor scaling all jet energies. We apply a cut to the peak value of individual event likelihoods in order to reduce the effect of badly reconstructed events. We report results based on a 1.7 fb^{-1} sample, using events with a lepton, large $\not\!\!E_T$, and exactly four high-energy jets in the pseudorapidity range $|\eta| < 2$. We require that at least one of the jets is tagged as coming from a b quark; 293 events pass all the selection criteria. We find $M_{\rm top} = 172.7 \pm 1.8$ (stat + JES) $\pm$ 1.2 (syst) GeV/c^2, or $M_{\rm top} = 172.7 \pm 2.1$ (tot) GeV/c^2.

Preliminary Results for Fall 2007 Conferences

I. INTRODUCTION

The top quark mass is an important parameter in the Standard Model, as a precision measurement of the top quark mass (along with the mass of the W boson) provides our best means for constraining the value of the Higgs boson mass. This note describes a precision measurement of the top quark mass performed using a matrix element integration method. For each event we obtain the likelihood of observing that event in our detector as a function of the true top mass m_t by integrating over seven kinematic variables and taking into account effects due to imperfectly known variables.

This analysis uses 1.7 fb^{-1} of data collected from $p\bar{p}$ collisions at the Fermilab Tevatron using the CDF II detector, as described in [1]. We search for events in which $t\bar{t}$ pairs are produced, each decays into a W boson and a b quark, and then one W decays into a neutrino and a lepton (meaning, in this paper, an electron or muon) and the other W decays into a $q\bar{q}'$ pair; this is called the "lepton + jets" channel.

We use a neural network constructed from a variety of event variables to distinguish between signal and bacgkround events, and employ a cut on the peak likelihood for a given event for additional rejection of background and poorly-modeled events.

The largest systematic uncertainty in the measurement of the top mass is due to uncertainties in the jet energy measurements. In our original measurement, we used a method to reduce jet systematics by calibrating the jet energy scale using the W mass constraint event-by-event [2]. A different method has been employed by other analyses [3–5] which consists in introducing a scale factor (JES) to scale the energies of all jets in the events of the sample. The information contained within each event about JES is used to determine an overall value of JES and an optimal value for the top mass. Most of the systematic uncertainties on the jet energy scale are thus included in the statistical uncertainty of the result. We used this method in our top mass measurement with 955 pb^{-1} [6], which this measurement is an update of.

II. DATA AND MONTE CARLO SAMPLES

In this analysis, we identify the top mass candidates in the lepton + jets channel by looking for four high energy jets from the four quarks and a W decay into a lepton and a neutrino. Specifically, for the lepton we require either an electron with $E_T > 20$ GeV or a muon with $p_T > 20$ GeV/c in the central region of the detector. The neutrino is identified by requiring a missing E_T ($\not\!\!E_T$) > 20 GeV in the event. For the jets, we require exactly 4 jets with $E_T > 20$ GeV and pseudorapidity $|\eta| < 2$. The jet p_T has been corrected for inhomogeneities of the detector and nonlinear response of the detector as a function of particle p_T. In addition, at least one of the jets must be tagged as a b-jet using a secondary vertex tagging algorithm.

Background to this signal consists of three main sources: events where a W is produced in conjunction with heavy flavor quarks ($b\bar{b}$, $c\bar{c}$, or c), events where a W is produced along with light quarks which are mistagged, and QCD events that do not contain a W boson but fake a lepton. There are also smaller contributions from diboson, Z, and single top events.

We use a variety of Monte Carlo samples in constructing and evaluating our method. For signal events, we use $t\bar{t}$ events generated at a variety of top masses from 152 GeV/c^2 to 190 GeV/c^2 using the PYTHIA Monte Carlo generator [7]. We also cross-check our analysis using $t\bar{t}$ signal events generated with the HERWIG generator [8]. For W+jets backgrounds, we use Monte Carlo events generated using ALPGEN [9] for the generator and PYTHIA to perform the parton shower. All Monte Carlo samples are then simulated using the CDFII simulation package. The non-W QCD background is derived from data; for the smaller contributions we do not use Monte Carlo samples, but rather increase the W+light flavor fraction to include diboson and Z contributions and increase the W+heavy flavor to include the single top contribution. Table I shows the individual contributions. For W+HF and W+LF the background was derived with the method used for the cross section measurement [10], where overlaps in the W+parton samples are removed using the ALPGEN jet-parton matching along with a jet-based heavy flavor overlap removal algorithm.

TABLE I: Expected backgrounds for the W+4 tight jet sample used.

Background	1 tag	$\geq$ 2 tags
non-W QCD	12.48 ± 10.76	0.42 ± 1.50
W+light mistag	14.52 ± 3.20	0.28 ± 0.08
diboson (WW, WZ, ZZ)	2.95 ± 0.24	0.24 ± 0.02
Z $\to ee, \mu\mu, \tau\tau$	1.72 ± 0.18	0.06 ± 0.01
Sum of above 3	19.19 ± 3.21	0.58 ± 0.08
W+bb	12.14 ± 4.90	2.46 ± 1.01
W+$c\bar{c}$, c	11.07 ± 4.50	0.51 ± 0.22
Single top	2.78 ± 0.17	0.83 ± 0.07
Sum of above 3	25.99 ± 9.13	3.80 ± 1.20
Total background	57.66 ± 14.88	4.80 ± 2.37
Events observed	263	80

We find that the total number of expected background events in our data sample is $N_{\text{background}} = 62.5 \pm 15.1$ events in 343 observed events.

III. METHOD

For each event we obtain a likelihood as a function of the top pole mass m_t and the jet energy scale JES using the following expression:

$$L = \frac{1}{N(m_t)} \frac{1}{A(m_t, \text{JES})} \sum_{i=1}^{24} w_i \int \frac{f(z_1) f(z_2)}{FF} \text{TF}(\vec{y} \cdot \text{JES} \mid \vec{x}) \, |M_{\text{eff}}(m_t, \vec{x})|^2 \, d\Phi(\vec{x}) \tag{1}$$

$$\text{with} \quad L = L(\vec{y} \mid m_t, \text{JES})$$

where $\vec{y}$ are the quantities we measure (the charged lepton and jet momenta); $\vec{x}$ are the parton-level quantities that define the kinematics of the event; $N(m_t)$ is a global normalization factor; JES is the previously-mentioned jet energy scale, an overall factor that multiplies the momentum of each jet; $A(m_t, \text{JES})$ is the acceptance as a function of m_t and JES; $f(z_1)$ and $f(z_2)$ are the momentum probability distributions, obtained from the PDFs, for incoming partons z_1 and z_2; FF is the flux factor for the PDF's; TF(JES $\cdot \vec{y} \mid \vec{x}$) are the transfer functions that predict the measured jet momenta distributions given the quark kinematics; d$\Phi(\vec{x})$ indicates integration over the phase space for the 6 partons in the $t\bar{t}$ decay (including necessary Jacobians); and $\text{M}_{\text{eff}}(m_t, \vec{x})$ is the modified matrix element for $t\bar{t}$ production and decay. The integral is calculated for each possible permutation of assigning jets to partons, and then summed with the appropriate weights w_i, where the weights are determined by the b-tagging information on the jets. In addition, for each event, we introduce a probability factor for the P_T of the $t\bar{t}$ system by integrating over a prior determined from the HERWIG Monte Carlo.

The PDFs $f(z_1)$ and $f(z_2)$ are integrated over the appropriate combinations of incoming $q\bar{q}$ and gluons. The flux factor acts as a normalization for the PDFs. We use the CTEQ5L PDFs [11] in our integration.

We discuss the further components of the integration in the following sections.

Matrix element: We use the Kleiss-Stirling matrix element [12] which includes both $q\bar{q} \to t\bar{t}$ and $gg \to t\bar{t}$ production processes, as well as all spin correlations.

Integration variables: The above formula would require a 22-dimensional integration (there are six momentum four-vectors for the decay products, and we know the lepton and neutrino

masses, leaving 22 unknowns). This is not computationally practical to evaluate, so we make some simplifying assumptions:

- The lepton angle and momentum are perfectly measured.
- The angles of the four quarks are perfectly measured by the jet angles.
- The hadronic b is on mass shell, the light quark masses are 0, and the leptonic b quark mass is also 0. This last assumption reduces the complexity of solving the leptonic-side kinematics from an 8th-order polynomial to a 4th-order polynomial, significantly reducing the computing time.

This leaves us with seven variables. We choose our set of variables to be the two M_t^2 and M_W^2 on the leptonic and hadronic side of the decay, $\beta = \log(p_1/p_2)$, where p_1 and p_2 are the scalar momenta of the two hadronic W decay products, and the two-dimensional vector p_T of the $t\bar{t}$ system.

Effective propagators: We integrate over the expected distributions of M_t^2 and M_W^2. These are the propagator terms in the matrix element, which are relativistic Breit-Wigners peaked at the nominal top and W mass. However, the assumptions described in the previous section cause the M_t^2 and M_W^2 distributions to be altered from their Breit-Wigner form. To account for this, we replace the Breit-Wigner propagators in the matrix element used in the integration with propagators which reflect the assumptions; we call these adjusted propagators "effective propagators".

In order to perform this adjustment, we first take our Monte Carlo events and create "effective partons". The "effective partons" have the same energy as the tree-level $t\bar{t}$ decay products, but their directions are set to the jet directions reconstructed in the detector and their masses satisfy the assumptions described in the previous section. We then construct the invariant mass distributions of these "effective partons" to obtain the M_t^2 and M_W^2 distributions used in our "effective propagators". On the hadronic side of the $t\bar{t}$ decay, the "effective propagators" depend on the event kinematics. We estimate the M_t^2 and M_W^2 covariance matrix due to errors in the determination of jet mass and direction (jet energy is excluded here), and use this matrix to look up an "effective propagator" pre-built from Monte Carlo events with similar properties. On the leptonic side we use an average effective propagator.

Examples of the hadronic and leptonic side "effective propagators" are shown in Figure 1. Note that the propagators are expressed in terms of ΔM_t, the difference between the pole top mass and the event top mass, thus allowing us to construct the propagators from samples with a wide range of true top mass values.

Transfer functions: The transfer functions connect the measured jets to the partons. They are probability distributions of the ratio of the magnitude of the jet momentum p to the parent "effective parton" energy E, parameterized as a function of the transverse momentum of the parent "effective parton" (described in the previous section). We construct our transfer functions by taking $t\bar{t} \rightarrow$ lepton + jets Monte Carlo events in a wide range of top masses, requiring the same selection cuts as described in Section II. From the events, the simulated jets are matched to their parent parton, different distributions of the resulting p/E values are created binned by the parent parton p_T, and then these distributions are fit with a p_T-parameterized function. The function is constructed using Johnson's functions, which allow us to fit possible non-Gaussian shapes for the transfer functions. We are also able to extrapolate the fit functions to momenta which are below the cutoff value. Separate transfer functions are created for four different η regions of the detector, as well as for b quarks and light quarks.

Figure 2 shows some sample fitted transfer functions for light and b quarks in different p_T and η bins.

Normalization: The normalization factor $N(m_t)$ is obtained by integrating the Kleiss-Sterling matrix element together with the PDF's and the flux factor over the phase space formed by the

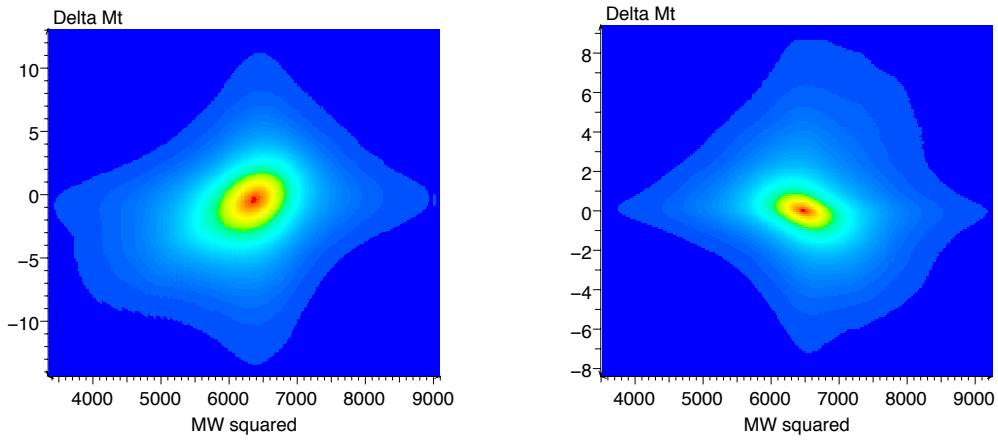

FIG. 1: Effective propagators used on the hadronic side (left) and leptonic side (right).

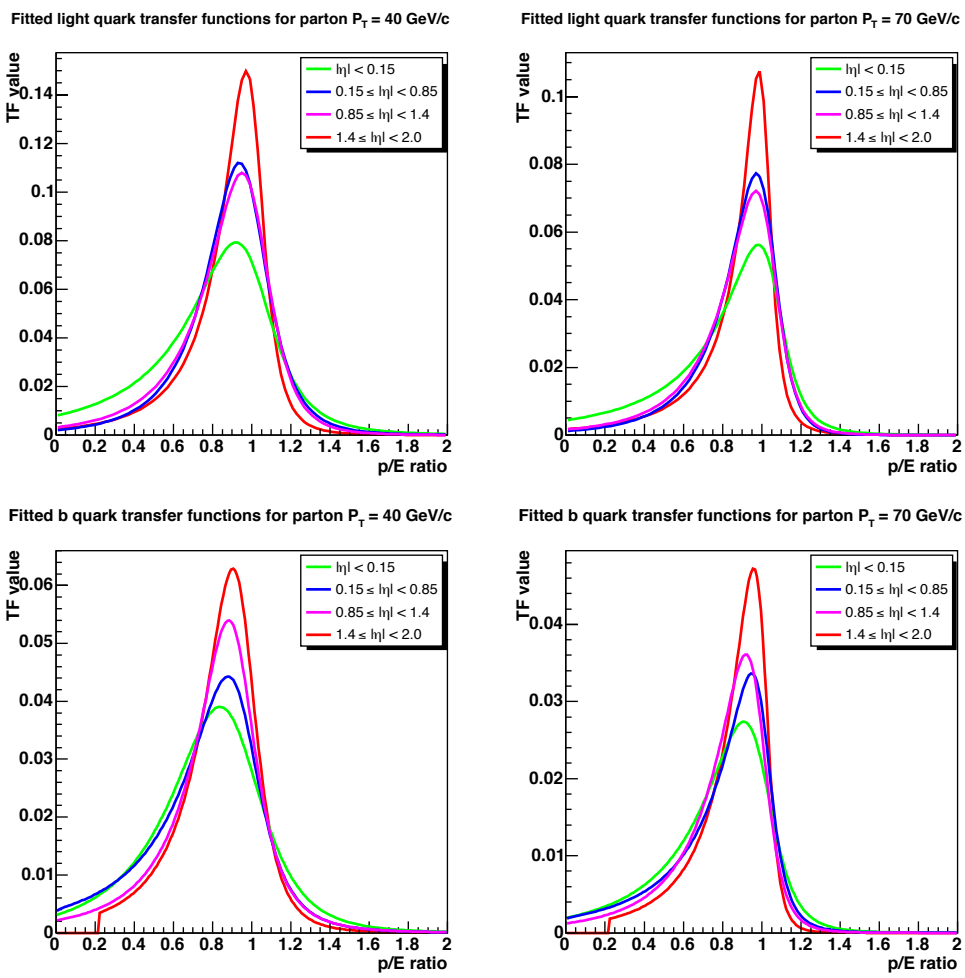

FIG. 2: Sample fitted transfer functions for light and b quarks in a variety of p_T and η bins.

two initial and the six final state particles. The resulting normalization is then corrected by a small additional factor to account for the difference between the effective propagators and Breit-Wigners.

Acceptance: The acceptance $A(m_t, \text{JES})$ is obtained from Monte Carlo events in which we take effective partons, randomize their angles to mimic the detector's angular resolution uncertainty, and randomize their momenta using our transfer functions to mimic the jet momenta which would have been measured in the detector. In this way, we create objects which should look like final-state jets. We do this for all the values of the top mass and JES over which the likelihood function is defined, and then calculate the acceptance at each m_t and JES value to be the fraction of these MC events which pass our selection cuts.

The advantage to this approach as opposed to using fully simulated Monte Carlo is that it does not have events with an incorrect set of jets, and such events are excluded from the efficiency calculations as well. Our probability model describes tree level signal events with the correct set of jets; therefore, we cannot use fully simulated events which include effects not included in the model. The transfer functions are normalized with respect to all jet momenta, not just those which pass the cuts. By building an acceptance off events whose jets assume our transfer functions are perfect, we directly normalize our transfer functions and therefore our likelihood. Furthermore, we can generate our acceptance from a much larger sample of events, reducing statistical fluctuations in the resulting curve. Figure 3 shows the 2-D acceptance as a function of m_t and JES.

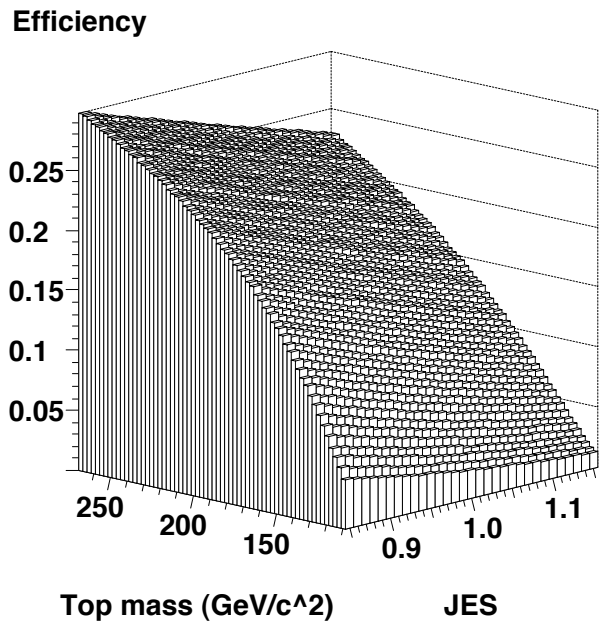

FIG. 3: Acceptance used in our integration.

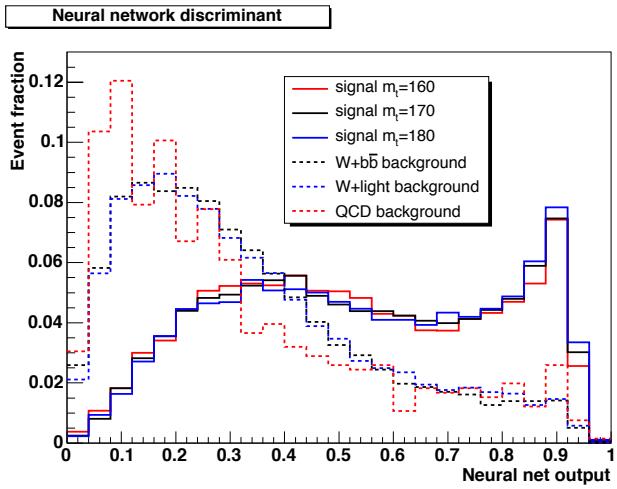

FIG. 4: The distributions of our hybrid variable for signal and background Monte Carlo events. The solid lines indicate signal events at various masses, while the dashed lines indicate various types of backgrounds.

IV. BACKGROUND DISCRIMINATION AND HANDLING

Our integration method calculates the likelihood for an event under the assumption that it is a signal event. Therefore, we need a mechanism to reject background events.

We identify background events using a neural network. Our neural network uses ten inputs: the P_T for each of the four leading jets; the E_T of the lepton; the missing E_T, $\not{E}_T$; H_T, the scalar sum of the jet transverse energies, lepton transverse energy, and missing E_T; and three variables describing the shape of the event: the aplanarity, defined as 3/2 the smallest eigenvalue of the momentum tensor $\Theta_{ab} = \sum_i p_a^i p_b^i / \sum_i |\vec{p_i}|^2$; $D_R = \Delta R_{ij}^{\min} \cdot \min(p_z^{(i,j)})/p_T^\ell$, where $\Delta R_{ij}^{\min}$ is the smallest ΔR between any pair of jets; and $H_{\mathrm{TZ}} = \sum_{i=2}^4 |p_T^i| / (\sum_{i=1}^4 |p_z^i| + |p_z^\ell| + |p_z^\nu|)$, the ratio of the scalar sums of the transverse momenta (excluding the leading jet) to the longitudinal momenta.

The neural network is trained to separate $t\bar{t}$ events with a mass of 170 GeV/c^2 and $W + b\bar{b}$ background; we then cross-check the neural network with other signal masses and background types to make sure that the output shape is not dependent on the signal mass present.

Figure 4 shows the neural network output for a variety of different samples. We then compute the background fraction for this event as $f_{\mathrm{bg}}(q) = B(q)/(B(q) + S(q))$, where the background and signal distributions are normalized to their overall expected fractions.

Next, we need to use this discriminant to remove the background contribution from our total likelihood to recover our signal likelihood. We compute the average likelihood for background events (computed, like all of our events, under the assumption that they are signal) from Monte Carlo and subtract out the expected contribution, where n_{bg} is the expected number of background events:

$$\log L_{\mathrm{tot}} = \sum_i (\log L_i) - n_{\mathrm{bg}} \log \overline{L(\mathrm{background})}$$

Since this background subtraction is not necessarily perfect, we also consider the possibility of "de-weighting" individual events using the background fraction obtained from our discriminant. We perform this de-weighting by averaging these curves with a uniform distribution U. So, for an individual event, we have:

$$\log L(m_t, \mathrm{JES}) \Rightarrow \log[L(m_t, \mathrm{JES})(1 - f_{\mathrm{bg}}(q)\kappa) + f_{\mathrm{bg}}(q)\kappa U]$$

In this equation, κ is an adjustable parameter we can tune to determine the optimal amount of de-weighting. However, in our studies, we determine that the optimum value of κ in this analysis is 0; that is, the benefits of de-weighting background events are always outweighed by the penalty from accidentally de-weighting signal events.

We can rewrite our previous equation in terms of the individual per-event background fraction to obtain our final likelihood formula:

$$\log L_{\rm mod}(m_t, \text{JES}) = \sum_{\text{events}} [\log L(m_t, \text{JES}\,|\text{signal}) - f_{bg}(q) \log \overline{L(m_t, \text{JES}\,|\text{background})}]$$

However, there is another class of undesirable events which is not handled by the above method. These are events which are $t\bar{t}$ signal, but where it's not the case that the four observed tight jets are produced by the four quarks in the $t\bar{t}$ decay. We call these events "bad signal" events. These exist due a variety of causes (extra jets from gluon radiation, misidentified dilepton or all-hadronic events, $W \to \tau$ decay, etc.) and comprise roughly 35% of our total signal (for a signal mass of 170 GeV/c^2, we see that 36.1% of 1-tag and 30.6% of >1-tag events are "bad signal"). In order to deal with these events, we implement a cut on the log of the value of the highest likelihood of the likelihood curve; we've optimized this value at 6, where Table II shows the efficiency of this cut for "good signal" events, "bad signal" events, and background events.

TABLE II: Efficiency of the likelihood cut at a value of 6.

Type of event	1-tag	>1-tag
Good signal	94.0%	96.4%
Bad signal	78.5%	78.3%
Background	71.1%	70.5%

V. TOP MASS EXTRACTION

Our 2-D likelihood gives us the joint likelihood of observing the events that we see as a function of the top mass m_t and the jet energy scale JES. In order to obtain a final result, we treat the JES as a nuisance parameter and eliminate it using the profile likelihood. In the profile likelihood method, we simply take the maximum value of the likelihood along the JES axis for each m_t value. That is:

$$L_{\rm prof}(m_t) = \max_{j \in \text{JES}} L(m_t, j)$$

This gives us a 1-D likelihood curve in m_t only. We then follow the normal procedure of taking the peak as our result and descending 1/2 unit of log-likelihood from the peak to determine the uncertainty.

We test our method using Monte Carlo samples of simulated $t\bar{t}$ events and the three major backgrounds, as described in section II. We construct pseudo-experiments (PEs) from the Monte Carlo using a Poisson average of 302.8 events per pseudo-experiment, the number of events we expect to have after applying the likelihood cut. We run 2000 PEs for each signal top mass value and compute the resulting average measured mass, bias, expected statistical uncertainty, and pull width. Figure 5 shows the results.

Based on the results from these PEs, we determine the calibration for our final measurement. From the bias plot, we adopt a correction of 1.22 ± 0.09 GeV/c^2 to our measured mass; this calibration appears to be independent of m_t, as the slope of the measured top mass versus the

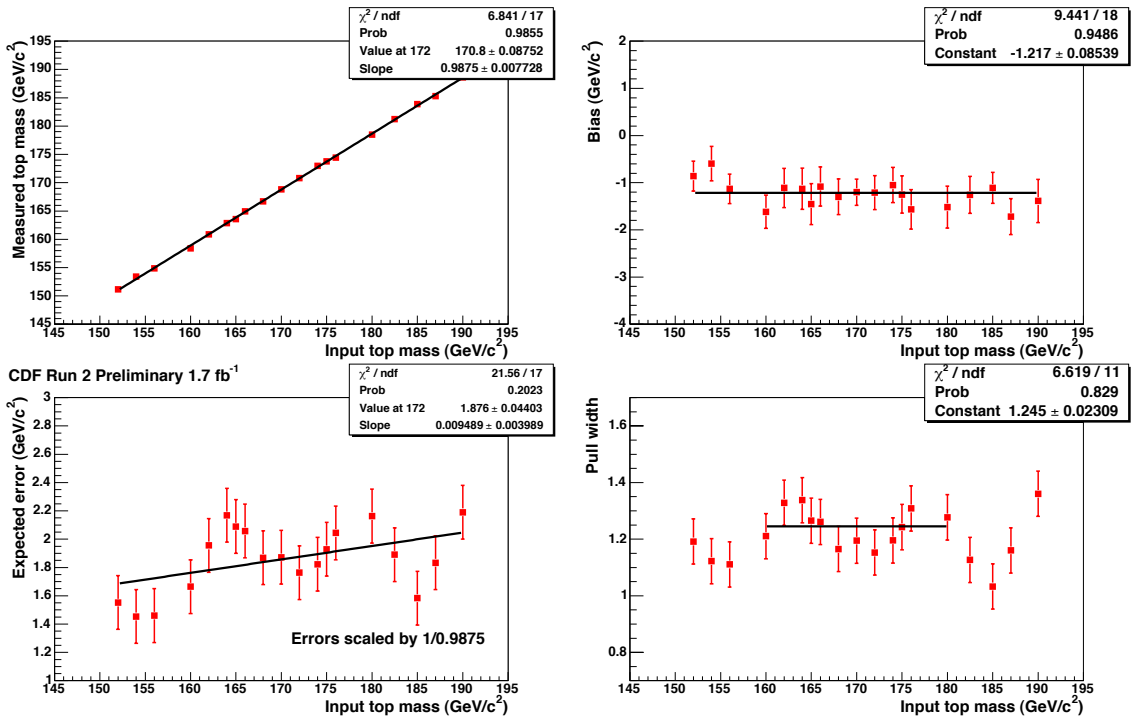

FIG. 5: Pseudoexperiment results using fully simulated signal and background events after applying a likelihood cut, mean of 302.8 events/PE. Top left: reconstructed vs. input top mass; top right: bias vs. input top mass; bottom left: expected uncertainty vs. input top mass; bottom right: pulls vs. input top mass.

input top mass is very close to 1. From the pull width, we apply a correction factor to our measured uncertainty of 1.245. Note that, due to concerns of the stability of our pull width with respect to m_t, we fit the pull width only in the range 160 to 180 GeV/c^2, which yields a somewhat higher result than fitting over the full range. We also use the measured slope of 0.988 to correct the resulting value and uncertainty.

To check that our 2-D likelihood method correctly handles changes in input JES, we also measure the top mass in samples in which the input JES has been shifted to different values. These plots are shown in Figure 6. We can see that the measured top mass is very stable with respect to input JES and that changing the input JES does not significantly affect the response slope or bias.

VI. RESULTS

In the data we find a total of 293 events which pass all of our cuts (including the likelihood peak cut): 219 1-tag events and 74 >1-tag events. Combining these likelihoods, we use the profile likelihood to extract a top mass value, which we then correct using the previously-described calibration, to measure a mass of 172.7 ± 1.8 GeV/c^2. Figure 7 shows the resulting 2-D likelihood from each subset of the events after the calibration has been applied.

This uncertainty combines both the statistical uncertainty and the uncertainty due to JES uncertainty. To separate these two causes, we take the m_t likelihood in the JES = 1 bin and evaluate the uncertainty in the resulting 1-D likelihood. This yields an uncertainty of 1.3 GeV/c^2. Thus, we conclude that the remaining uncertainty of 1.2 GeV/c^2 is due to the JES and report a final value of:

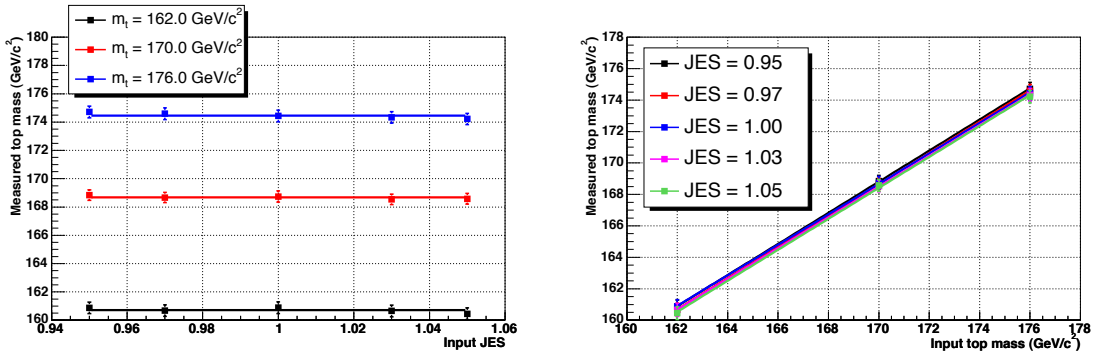

FIG. 6: Results of our JES cross-checks. Left: reconstructed top mass vs. input JES for three different top mass values. Right: reconstructed top mass vs. input top mass for five different JES values.

$$M_{\rm top} = 172.7 \pm 1.3 \text{ (stat.)} \pm 1.2 \text{ (JES) GeV}/c^2. \tag{2}$$

Figure 8 shows the expected statistical uncertainty from Monte Carlo events at a top mass of 172 GeV/c^2, with the measured uncertainty from data shown as the black arrow. 34% of pseudoexperiments show a lower uncertainty than measured in the data.

As a cross-check, Figure 9 shows the comparison of the likelihood information between data and Monte Carlo. The left plot shows the m_t location of the peak of the individual likelihood curves, while the right plot shows the log-likelihood value of the likelihood curve at its peak. Note that the left plot includes only events that pass the likelihood cut; the right plot, obviously, includes all events. In both cases we see excellent agreement between the two. The right plot is especially important because it indicates that the likelihood peak information is well-modeled by Monte Carlo and hence the likelihood cut that we apply will be valid.

Our systematics are summarized in Table III. Here is a brief description of the major systematic sources:

While the 2-D measurement is designed to capture any changes in the JES, we use a single flat factor for the jet energy scale, while the jet energy systematic uncertainties depend on the jet p_T and η. To evaluate potential systematics from this, for each source of systematic uncertainty in the jet energy, we shift the jet energies by one σ for that uncertainty. The resulting shifts are added in quadrature to obtain our residual JES systematic uncertainty.

We evaluate the systematics due to the parton distribution functions (PDFs) used in the matrix element integration by comparing different PDF sets (CTEQ5L and MRST72 [13]), varying α_s, and varying the eigenvectors of the CTEQ6M PDFs.

Systematics due to initial-state radiation and final-state radiation are evaluated using Monte Carlo samples where the amount of ISR and FSR has been increased and decreased.

Our analysis is tested and calibrated on PYTHIA Monte Carlo, while many of its internal components are created using HERWIG Monte Carlo. We evaluate a systematic due to the generator by comparing the results from HERWIG and PYTHIA samples.

There are several uncertainties associated with our background method. First, we vary our overall background fraction by its uncertainty and measure the resulting change in the top mass. Second, we check the background composition by setting our background to 100% $W+b\bar{b}$, $W+c\bar{c}/c$, W + light, or QCD background and measuring the resulting changes. Third, we check the systematics due to our average background likelihood shape by dividing the sample into two subsamples (one with electrons, and one with muons), building the average shape from one subsample, and measuring the top mass on the other subsample. Finally, we use background samples with a different Q^2 scale used by the Monte Carlo generator to evaluate the systematics due to this source.

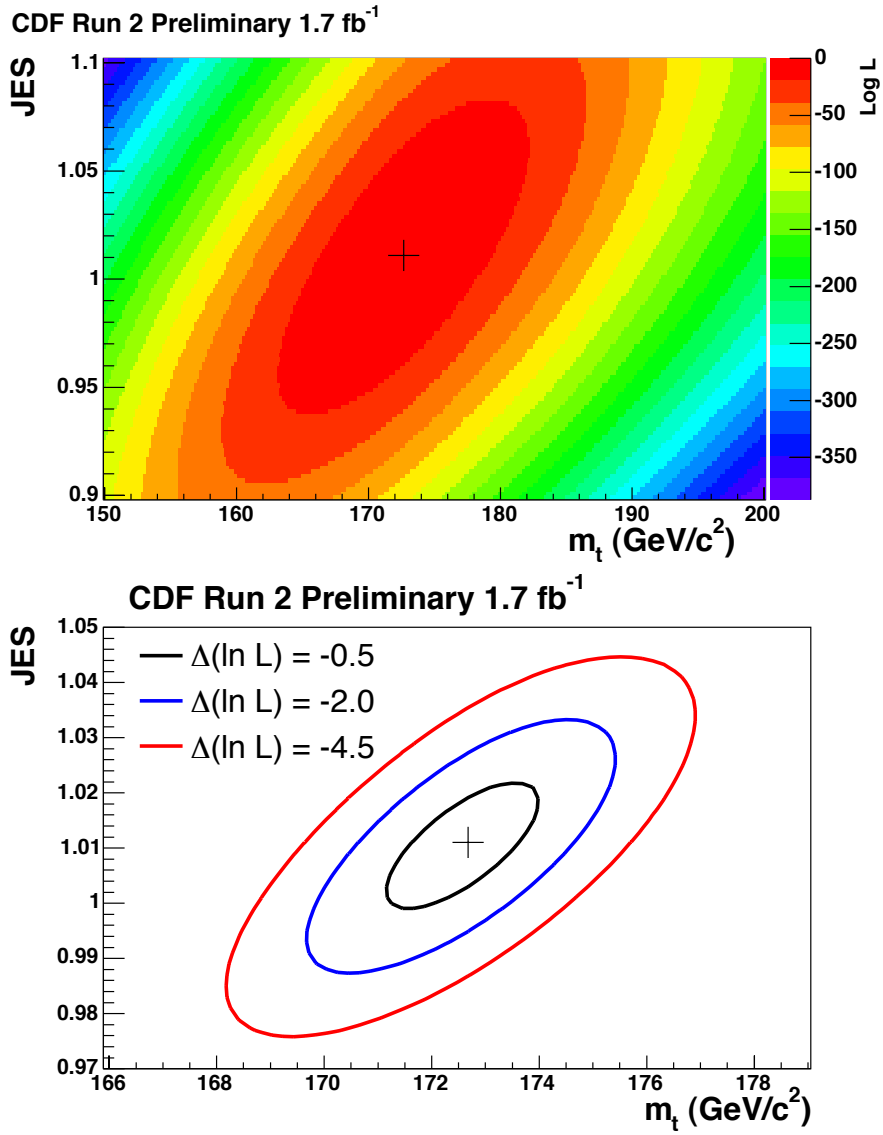

FIG. 7: Measured 2-D likelihood on the data events. The top plot shows the likelihood on the full range used in our integration. The bottom plot shows the contours corresponding to a 1-σ, 2-σ, and 3-σ uncertainty in our measurement. The calibration derived from Monte Carlo has been applied to the top mass; the JES is uncalibrated. The marker shows the point of maximum likelihood.

We have estimated from Monte Carlo an additional 0.6% uncertainty on the jet energy scale for b jets due to uncertainties in b fragmentation and semileptonic decays. Thus, we vary the b-jets alone by this amount and measure the resulting systematic on the top mass. We also have small systematics resulting from the dependence of the b-tagging efficiency on jet E_T, the permutation weighting used in our integration, multiple interactions, and uncertainty in the lepton P_T.

VII. CONCLUSIONS

In conclusion, our measured top quark mass in 1.7 fb^{-1} with 293 events passing all our cuts is:

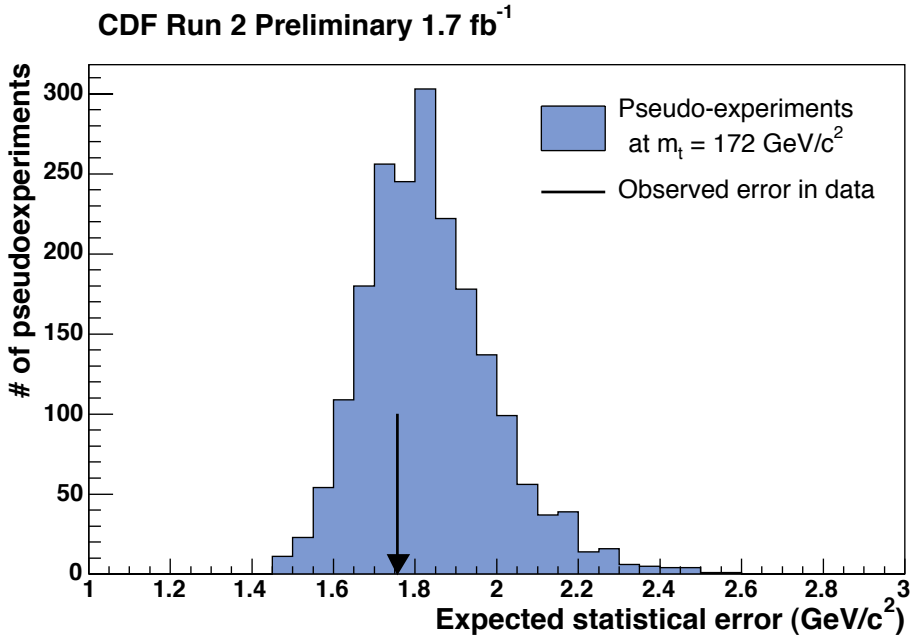

FIG. 8: Expected statistical uncertainty on the 2-D profile likelihood method for $m_t = 172$. The black arrow indicates the measured uncertainty in data. All uncertainties have been scaled by the average pull width of 1.245.

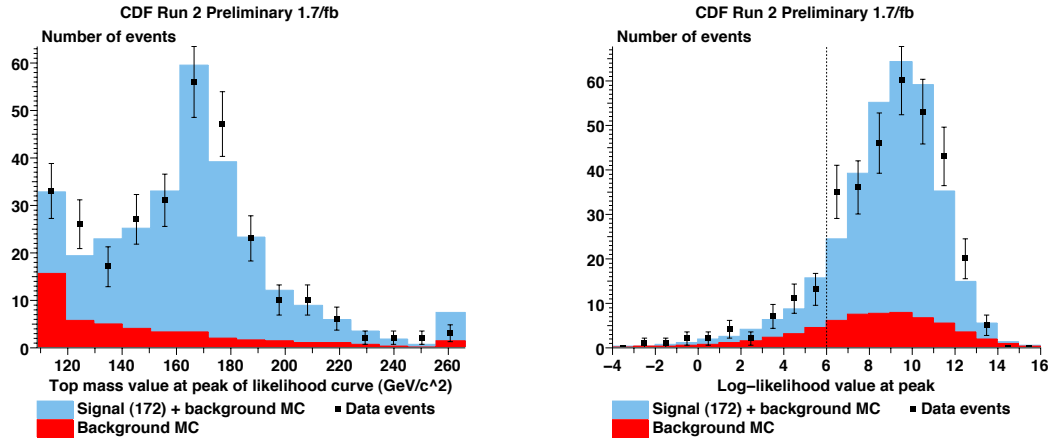

FIG. 9: Comparison of the likelihood curves for data and Monte Carlo. Left: m_t position of the peak of individual likelihood curves which pass the likelihood cut. Right: Log-likelihood value of the peak of individual likelihood curves.

$$M_{\rm top} = 172.7 \pm 1.3 \text{ (stat.)} \pm 1.2 \text{ (JES)} \pm 1.2 \text{ (syst.) GeV}/c^2$$
$$M_{\rm top} = 172.7 \pm 1.3 \text{ (stat.)} \pm 1.7 \text{ (syst.)} = 172.7 \pm 2.1 \text{ (total) GeV}/c^2.$$

Acknowledgments

We thank the Fermilab staff and the technical staffs of the participating institutions for their vital contributions. This work was supported by the U.S. Department of Energy and National

TABLE III: Total list of systematics.

Systematic source	Systematic uncertainty (GeV)
Calibration	0.09
MC generator	0.19 ± 0.36
ISR	0.26 ± 0.37
FSR	0.13 ± 0.38
Residual JES	0.53
b-JES	0.36
Lepton P_T	0.11
Permutation weighting	0.03
Multiple interactions	0.05
PDFs	0.25
Background: fraction	0.33
Background: composition	0.39
Background: average shape	0.31
Background: Q^2	0.07 ± 0.20
Gluon fraction	0.14
b-tag E_T dependence	0.16
Total	1.16

Science Foundation; the Italian Istituto Nazionale di Fisica Nucleare; the Ministry of Education, Culture, Sports, Science and Technology of Japan; the Natural Sciences and Engineering Research Council of Canada; the National Science Council of the Republic of China; the Swiss National Science Foundation; the A.P. Sloan Foundation; the Bundesministerium für Bildung und Forschung, Germany; the Korean Science and Engineering Foundation and the Korean Research Foundation; the Science and Technology Facilities Council and the Royal Society, UK; the Institut National de Physique Nucleaire et Physique des Particules/CNRS; the Russian Foundation for Basic Research; the Comisión Interministerial de Ciencia y Tecnología, Spain; the European Community's Human Potential Programme; the Slovak R&D Agency; and the Academy of Finland.

[1] F. Abe, et al., Nucl. Instrum. Methods Phys. Res. A **271**, 387 (1988); D. Amidei, et al., Nucl. Instum. Methods Phys. Res. A **350**, 73 (1994); F. Abe, et al., Phys. Rev. D **52**, 4784 (1995); P. Azzi, et al., Nucl. Instrum. Methods Phys. Res. A **360**, 137 (1995); The CDFII Detector Technical Design Report, Fermilab-Pub-96/390-E

[2] The CDF Collaboration, "Top Mass Measurement in the Lepton + Jets Channel using a Multivariate Template Method", CDF public note 7102 (July 2004).

[3] The CDF Collaboration, "Measurement of the Top Quark Mass using the Matrix Element Analysis Technique in the Lepton + Jets Channel with In-Situ $W \to jj$ Calibration", CDF public note 8151 (March 2006).

[4] The CDF Collaboration, "Measurement of the Top Quark Mass using the Template Method in the Lepton plus Jets Channel with *In Situ* $W \to jj$ Calibration", CDF public note 8125 (March 2006).

[5] The CDF Collaboration, "Measurement of the top quark mass in the all hadronic channel using an in-situ calibration of the dijet invariant mass with 943 pb^{-1}", CDF public note 8709 (February 2007).

[6] The CDF Collaboration, "Top Mass Measurement in the Lepton + Jets Channel Using a Multivariate Method and *in situ* Jet Calibration", CDF public note 8780 (April 2007).

[7] PYTHIA version 6.216, T. Sjöstrand, P. Edén, C. Friberg, L. Lönnblad, G. Miu, S. Mrenna and E. Norrbin, Computer Phys. Commun. 135 (2001) 238 (LU TP 00-30, hep-ph/0010017).

[8] HERWIG version 6.510, G. Corcella, I.G. Knowles, G. Marchesini, S. Moretti, K. Odagiri, P. Richardson, M.H. Seymour and B.R. Webber, JHEP 0101 (2001) 010 [hep-ph/0011363]; hep-ph/0210213.

[9] ALPGEN version 2.10 prime, M.L. Mangano, M. Moretti, F. Piccinini, R. Pittau, A. Polosa, JHEP 0307:001,2003, hep-ph/0206293. Note that PYTHIA v6.325 is used for the showering.

[10] The CDF Collaboration, "Measurement of the $t\bar{t}$ Production Cross Section in $p\bar{p}$ collisions at $\sqrt{s} = 1.96$ TeV using Lepton + Jets Events with Secondary Vertex b-tagging", CDF public note 8795 (May 2007).
[11] H. L. Lai *et al.*, Eur. Phys. J. C **12**, 375 (2000).
[12] R. Kleiss and W. J. Stirling, Z. Phys. C **40**, 419 (1988).
[13] A. D. Martin, R. G. Roberts, W. J. Stirling and R. S. Thorne, Eur. Phys. J. C **4**, 463 (1998).